Biomedical Optics EXPRESS

Multispectral scanning time-resolved fluorescence spectroscopy (TRFS) technique for intravascular diagnosis

Hongtao Xie,[1] Julien Bec,[1] Jing Liu,[1] Yang Sun,[1] Matthew Lam,[1] Diego R. Yankelevich,[1] and Laura Marcu[1,*]

[1]*University of California, Davis, Department of Biomedical Engineering, 451 Health Sciences Drive, Davis, CA 95616, USA*

**lmarcu@ucdavis.edu*

Abstract: This study describes a scanning time-resolved fluorescence spectroscopy (TRFS) system designed to continuously acquire fluorescence emission and to reconstruct fluorescence lifetime images (FLIM) from a luminal surface by using a catheter-based optical probe with rotary joint and pull-back device. The ability of the system to temporally and spectrally resolve the fluorescence emission from tissue was validated using standard dyes and tissue phantoms (e.g., *ex vivo* pig aorta phantom). Current results demonstrate that this system is capable to reliably resolve the fluorescence emission of multiple fluorophores located in the lumen; and suggest its potential for intravascular detection of distinct biochemical features of atherosclerotic plaques.

OCIS codes: (170.6510) Spectroscopy, tissue diagnostics; (300.6500) Spectroscopy, time-resolved; (110.7170) Ultrasound; (170.6935) Tissue characterization.

References and links

1. P. R. Moreno and J. E. Muller, "Identification of high-risk atherosclerotic plaques: a survey of spectroscopic methods," Curr. Opin. Cardiol. **17**(6), 638–647 (2002).
2. Y. Honda and P. J. Fitzgerald, "Frontiers in intravascular imaging technologies," Circulation **117**(15), 2024–2037 (2008).
3. P. Uehlinger, T. Gabrecht, T. Glanzmann, J. P. Ballini, A. Radu, S. Andrejevic, P. Monnier, and G. Wagnières, "In vivo time-resolved spectroscopy of the human bronchial early cancer autofluorescence," J. Biomed. Opt. **14**(2), 024011 (2009).
4. K. König, "Clinical multiphoton tomography," J Biophotonics **1**(1), 13–23 (2008).
5. M. Y. Berezin and S. Achilefu, "Fluorescence lifetime measurements and biological imaging," Chem. Rev. **110**(5), 2641–2684 (2010).
6. P. A. De Beule, C. Dunsby, N. P. Galletly, G. W. Stamp, A. C. Chu, U. Anand, P. Anand, C. D. Benham, A. Naylor, and P. M. French, "A hyperspectral fluorescence lifetime probe for skin cancer diagnosis," Rev. Sci. Instrum. **78**(12), 123101 (2007).
7. L. Marcu, "Fluorescence lifetime in cardiovascular diagnostics," J. Biomed. Opt. **15**(1), 011106 (2010).
8. L. Marcu, M. C. Fishbein, J. M. Maarek, and W. S. Grundfest, "Discrimination of human coronary artery atherosclerotic lipid-rich lesions by time-resolved laser-induced fluorescence spectroscopy," Arterioscler. Thromb. Vasc. Biol. **21**(7), 1244–1250 (2001).
9. L. Marcu, J. A. Jo, Q. Fang, T. Papaioannou, T. Reil, J. H. Qiao, J. D. Baker, J. A. Freischlag, and M. C. Fishbein, "Detection of rupture-prone atherosclerotic plaques by time-resolved laser-induced fluorescence spectroscopy," Atherosclerosis **204**(1), 156–164 (2009).
10. J. Phipps, Y. Sun, R. Saroufeem, N. Hatami, M. C. Fishbein, and L. Marcu, "Fluorescence lifetime imaging for the characterization of the biochemical composition of atherosclerotic plaques," J. Biomed. Opt. **16**(9), 096018 (2011).
11. D. N. Stephens, J. Park, Y. Sun, T. Papaioannou, and L. Marcu, "Intraluminal fluorescence spectroscopy catheter with ultrasound guidance," J. Biomed. Opt. **14**(3), 030505 (2009).
12. Y. Sun, R. Liu, D. S. Elson, C. W. Hollars, J. A. Jo, J. Park, Y. Sun, and L. Marcu, "Simultaneous time- and wavelength-resolved fluorescence spectroscopy for near real-time tissue diagnosis," Opt. Lett. **33**(6), 630–632 (2008).

#166495 - $15.00 USD Received 13 Apr 2012; revised 25 May 2012; accepted 25 May 2012; published 6 Jun 2012

13. Y. Sun, Y. Sun, D. Stephens, H. Xie, J. Phipps, R. Saroufeem, J. Southard, D. S. Elson, and L. Marcu, "Dynamic tissue analysis using time- and wavelength-resolved fluorescence spectroscopy for atherosclerosis diagnosis," Opt. Express **19**(5), 3890–3901 (2011).
14. "American National Standard for Safe Use of Lasers," ANSI Z136.1-2007 (ANSI, 2007).
15. "Using FastFrame segmented memory," Application note (Tektronix).
16. D. Magde, G. E. Rojas, and P. G. Seybold, "Solvent dependence of the fluorescence lifetimes of xanthene dyes," Photochem. Photobiol. **70**(5), 737–744 (1999).
17. H. Pal, S. Nad, and M. Kumbhakar, "Photophysical properties of coumarin-120: Unusual behavior in nonpolar solvents," J. Chem. Phys. **119**(1), 443–452 (2003).
18. G. Jones II, W. R. Jackson, C. Choi, and W. R. Bergmark, "Solvent effects on emission yield and lifetime for Coumarin laser dyes: requirements for a rotatory decay mechanism," J. Phys. Chem. **89**(2), 294–300 (1985).
19. N. Boens, W. W. Qin, N. Basarić, J. Hofkens, M. Ameloot, J. Pouget, J. P. Lefèvre, B. Valeur, E. Gratton, M. vandeVen, N. D. Silva, Jr., Y. Engelborghs, K. Willaert, A. Sillen, G. Rumbles, D. Phillips, A. J. W. G. Visser, A. van Hoek, J. R. Lakowicz, H. Malak, I. Gryczynski, A. G. Szabo, D. T. Krajcarski, N. Tamai, and A. Miura, "Fluorescence lifetime standards for time and frequency domain fluorescence spectroscopy," Anal. Chem. **79**(5), 2137–2149 (2007).
20. M. Arık, N. Celebi, and Y. Onganer, "Fluorescence quenching of fluorescein with molecular oxygen in solution," J. Photochem. Photobiol. Chem. **170**(2), 105–111 (2005).
21. A. Žukauskas, P. Vitta, N. Kurilcik, S. Jursenas, and E. Bakiene, "Characterization of biological materials by frequency-domain fluorescence lifetime measurements using ultraviolet light-emitting diodes," Opt. Mater. **30**(5), 800–805 (2008).
22. J. Liu, Y. Sun, J. Qi, and L. Marcu, "A novel method for fast and robust estimation of fluorescence decay dynamics using constrained least-squares deconvolution with Laguerre expansion," Phys. Med. Biol. **57**(4), 843–865 (2012).
23. J. A. Jo, Q. Fang, T. Papaioannou, and L. Marcu, "Fast model-free deconvolution of fluorescence decay for analysis of biological systems," J. Biomed. Opt. **9**(4), 743–752 (2004).
24. Y. Sun, J. Park, D. N. Stephens, J. A. Jo, L. Sun, J. M. Cannata, R. M. Saroufeem, K. K. Shung, and L. Marcu, "Development of a dual-modal tissue diagnostic system combining time-resolved fluorescence spectroscopy and ultrasonic backscatter microscopy," Rev. Sci. Instrum. **80**(6), 065104 (2009).
25. J. Pu, G. S. Mintz, E. S. Brilakis, S. Banerjee, A. R. Abdel-Karim, B. Maini, S. Biro, J. B. Lee, G. W. Stone, G. Weisz, and A. Maehara, "In vivo characterization of coronary plaques: novel findings from comparing greyscale and virtual histology intravascular ultrasound and near-infrared spectroscopy," Eur. Heart J. **33**(3), 372–383 (2012).
26. J. Bec, H. Xie, D. Yankelevich, F. Zhou, Y. Sun, N. Ghata, R. Aldredge, and L. Marcu, "Design, construction and validation of a multimodal intravascular diagnostic catheter combining IVUS and fluorescence lifetime spectroscopy detection channels," Proc. SPIE **7883**, 788337 (2011).

1. Introduction

Advances in the diagnosis of atherosclerotic cardiovascular disease depend on the availability of tools for the characterization of arterial wall and reliable detection and discrimination of distinct types of plaques [1,2]. Time-resolved (lifetime) fluorescence techniques have demonstrated potential tissue diagnosis including cancer [3–6] and atherosclerotic plaques [7]. Recent reports showed that instrumentation based on either time-resolved fluorescence spectroscopy (TRFS) or fluorescence lifetime imaging (FLIM) techniques can generate useful label-free optical molecular contrast for detection of critical atherosclerotic plaque such as plaques with thin fibrous cap [8], plaques rich in lipids [9,10], and plaques with macrophage infiltration in the fibrotic cap [9]. These lifetime techniques exploit the autofluorescence properties of several intrinsic constituents including elastin, collagen, and lipids in normal and diseased arterial walls in order to characterize the biochemical composition of atherosclerotic plaques [7]. Nevertheless, virtually all current TRFS and FLIM studies in arterial vessels have been conducted in *ex vivo* tissue specimens or *in vivo* during vascular procedures where the plaque is directly exposed to optical interrogation (e.g., during endarterectomy). Practical application of these techniques requires development of catheters that facilitate for the intravascular interrogation of the arterial wall [11]. Therefore, the development of a practical catheter-based intravascular TRFS system is critical for the clinical application of this technique.

In this paper, we report the development of a catheter-based scanning-TRFS system that allows for the intravascular reconstruction of spectroscopic fluorescence intensity and lifetime images (FLIM) of the luminal surface. A simultaneous rotation and pull-back of a side-

#166495 - $15.00 USD Received 13 Apr 2012; revised 25 May 2012; accepted 25 May 2012; published 6 Jun 2012

viewing fiber optic is used to generate a helical scan of the arterial wall. This enables reconstruction of fluorescence intensity and fluorescence lifetime images of any arterial segment. In each image, the "pixel" size is defined by the catheter scanning speed, the numerical aperture of the fiber optic, and the distance between fiber and lumen. Furthermore generation of hyperspectral FLIM images is achieved by coupling this scanning approach to a spectroscopic device designed to simultaneously resolve the fluorescence decay profile in multiple spectral bands; a technique previously reported by our group [12,13]. Specifically, the goals of current study are a) to validate the performance of the helical scanning-TRFS system by quantifying the effect of scanning speed and fiber-to-sample distance (or working distance) on data recording and spatial resolution of the system and b) to determine whether the spectral lifetime signature of samples (fluorescence dyes and tissue samples) previously interrogated using single point spectroscopy can be also retrieved using the scanning-TRFS.

2. Materials and methods

2.1 Scanning-TRFS system

2.1.1 Scanning-TRFS system configuration

The schematic diagram of the scanning-TRFS system is shown in Fig. 1. A pulsed nitrogen laser operating at 30 Hz was used as the fluorescence excitation source (337 nm, pulse width 700 ps). A side-viewing optical fiber (SVOF) rotating inside of a sheath and connected to a rotary joint allowed for coupling of the excitation beam or the fluorescence light and the sample. The distal end of the fiber optic was polished to 45° and coated with aluminum to deliver excitation and collect fluorescence emission from the vessel lumen (90° from the fiber axis). The proximal end of the fiber was enclosed in a 22 Gauge stainless steel tube as a ferrule, tightened to a shaft. This shaft was connected by mean of a belt/pulley assembly to a brushless motor drive with an integrated closed loop controller for precise rotation control (maximum speed 12000 rpm, Maxon compact drive EPOS 60W). It was verified that the fiber used was torsionally stiff enough as none of the acquired data presents nonuniform rotation distortion (NURD) artifacts. The pull-back motion was achieved by connecting the protection sheath to a translation stage (model 860SC-C, Newport), allowing a precise translation without interfering with the rotation.

A wavelength selection module allowed for simultaneous acquisition of fluorescence decay profiles in four spectral bands based on a principle previously described [12]. This module consisted of a set of dichroic filters and band-pass filters allowing for selection of four channels or wavelength bands (central wavelength/bandwidth): channel 1 (390/40 nm),

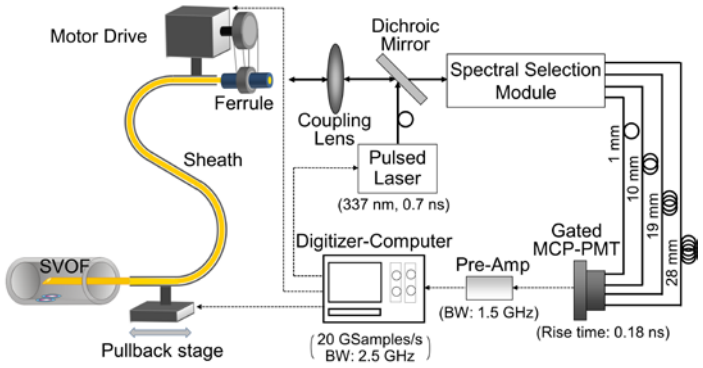

Fig. 1. Schematic of the helical (radial) scanning-TRFS system depicting the SVOF running in a lumen. Solid line shows the optical pathway while the dotted line shows the electronic control. The spectral selection module consists of a set of dichroic filters and band-pass filters allowing for selection of four wavelength bands (central wavelength/bandwidth): channel 1 (390/40 nm), channel 2 (452/45 nm), channel 3 (542/50 nm) and channel 4 (629/53 nm).

#166495 - $15.00 USD Received 13 Apr 2012; revised 25 May 2012; accepted 25 May 2012; published 6 Jun 2012

channel 2 (452/45 nm), channel 3 (542/50 nm) and channel 4 (629/53 nm). Each channel was coupled to optical fibers of different lengths acting as optical delay lines. Consequently the spectrally resolved fluorescence pulses arrived to the detector separated in time (47 ns time delay between pulses). The fluorescence detection module included a fast-gated multichannel plate photomultiplier tube (MCP-PMT) (rise time 0.18 ns, R5916U-50, Hamamatsu), a preamplifier (bandwidth 1.5 GHz, 36 dB, C5594-12, Hamamatsu), and a high speed digital oscilloscope (20 Gsamples/s, bandwidth 2.5 GHz, DPO 7254, Tektronix) for digitization of signals. A customized program written in LabVIEW was used to control the trigger, scanning, and data acquisition tasks.

This system was primarily designed for testing the acquisition of fluorescence map data from a helical scan of circular surfaces. However, it can be also used for linear scanning of planar surfaces as previously reported [13]. In this previous report, a XY-linear scan was implemented by using a PC-controlled xyz-motorized stage (1 μm resolution, MX80L and MX80S, Parker-Daedal). In current study we used a linear scanning setup to determine the effect of the scanning speed on the imaging resolution of the system, which will be later used to compare the effects of helical scanning on system performance in a tubular structure.

In present configuration, the energy at the laser output port as measured with a power meter (PD10-SH-V2, Ophir-Spiricon) was 10 μJ/pulse. Energy of the excitation light at the tip of the side-viewing optical fiber was measured as 2 μJ/pulse, resulting in a 20% transmission efficiency. During the experiments, the energy of the incident light delivered to sample was kept constant at 2 μJ/pulse (fluence of 0.16 mJ/cm^2 for 400 μm fiber in contact with tissue surface), which is below the ANSI limit for Maximum Permissible Exposure of UV light exposure of for skin (3 mJ/cm^2) [14].

2.1.2 FastFrame data acquisition

The FastFrame segmented memory feature of the digital oscilloscope was utilized for data acquisition [15]. This feature facilitated the fastest trigger rate of 400,000 frames per second (acquisitions/sec) with only a maximum dead time of 2.5 μs compared to that of 13 ms in the normal acquisition mode; and it can be adapted for the purpose of fast data acquisition with effective analysis and storage of data. For the 2D-helical scan, unless otherwise specified, all fluorescence data were recorded with the FastFrame acquisition mode (7000 acquisition frames with 4000 samples/frame).

2.2 Phantom preparation

2.2.1 Standard fluorescence dyes

To characterize and validate the scanning system, a series of measurements were taken with standard fluorescence dyes which have well-characterized fluorescence lifetimes. These include: 0.1 M Rhodamine B (RhB) in ethanol (emission peak 600 nm, lifetime 2.5-3.0 ns [16]), 0.1 M coumarin-120 (C120) in ethanol (emission peak 430 nm, lifetime 3.64 ns [17]), 0.1 M coumarin-1 (C1) in ethanol (emission peak 450 nm, lifetime 3.1 ns [18]), 9-cyanoanthracene (9CA) in PBS (emission peak 445 nm, lifetime 11.9 ns [19]), and fluorescein isothiocyanate (FITC) in PBS (emission peak 540 nm, lifetime 3.6 ns [20]). The emission wavelengths of these dyes covered the four wavelength bands of the scanning TRFS system and provide a range of lifetime values from 2.5 ns to 12 ns.

2.2.2 Polymerization of dye solution

In order to mount fluorescence targets into a phantom, it was necessary to fix the dye solution into a solid state. This was achieved by mixing the dye solution with SiO_2 powder (mean diameter 5 μm, Sigma-Aldrich) and an optical adhesive (optically transparent, NOA 88, Norland). The latter showed weak fluorescence at 337 nm. The mixture was then siphoned into capillary tubes and cured into a solid state with UV light exposure. Borosilicate glass

#166495 - $15.00 USD Received 13 Apr 2012; revised 25 May 2012; accepted 25 May 2012; published 6 Jun 2012

capillary (ID 0.5 mm, OD 1 mm, Sutter Instrument) was used to maintain fluorophore geometry in circular shape with a diameter of 0.5 mm.

2.2.3 Physical phantoms

Four types of physical phantoms were built to test the following imaging system properties: (Phantom 1) To characterize the effect of scanning speed on the pixel size of images in linear scanning, a pair of capillaries with RhB solution was cured, positioned 0.5 mm apart (distance between the capillary edges), and embedded in a nonfluorescent rectangular agar phantom. (Phantom 2) To characterize the effect of vessel diameter on helical scanning pixel size, a pair of capillaries with RhB were cured, positioned 0.5 mm apart along the circumference, and mounted on acrylic tubes with lumen diameters of 2, 4 and 6 mm, respectively. (Phantom 3) To determine the spatial resolution of the scanning system (i.e., the smallest target the scanning-TRFS system can resolve), a capillary tube was stretched into a sharp-tipped by pulling the glass capillary with a micropipette puller (Sutter Instruments), providing an imaging target with a gradually decreasing diameter of 500 μm to 80 μm. RhB was cured in the capillary with varied-diameters. (Phantom 4) To validate the ability of the system to resolve lifetime characteristics of fluorophores in multiple spectral bands, five fluorescent dyes (C120, C1, 9CA, FITC and RhB) were cured in capillaries and radially mounted into an acrylic tube with lumen diameter of 6 mm.

2.2.4 Pig aorta phantom

A hybrid tissue phantom was generated to determine whether the scanning-TRFS system is sensitive enough to resolve the autofluorescence emission of the normal arterial wall rich in elastin as well as to evaluate its ability to resolve markers with distinct features (e.g., composition or structure) from the arterial wall fluorescent background, This includes the ability of the scanning system to resolve fluorophores with short lifetime (comparable with that of lipid constituents) from normal arterial tissue. A segment of *ex vivo* pig aorta sample was harvested from a freshly excised pig heart, providing fluorescence signal of elastin (emission peak 410 nm, lifetime 5.2-7.4 ns [21]). Two fluorophore beads (size 1x1x1 mm^3) containing C1 and FITC respectively were fabricated using the polymerization procedure described in section 2.2.2, and subsequently placed on a stent (6 mm, Express Biliary LD, Boston Scientific). The stent was then deployed inside of the pig aorta. This approach allowed for the creation of target landmarks on intact normal arterial wall as well as for preservation of the round lumen shape. During scanning the hybrid tissue phantom was placed in saline.

2.3 System characterization and validation

2.3.1 Pixel size in XY-linear scan

XY-linear scanning was performed along an "S" shaped scanning pattern using a PC-controlled xyz-motorized stage. The pixel size in the scanning direction (i.e., x-direction, Δx) was defined as the scanning distance during the time interval required to acquire, average, and store 6 consecutive fluorescence responses. This time interval was roughly 0.4 s (with negligible error around 0.001 s), which was assumed to be constant for the purpose of this study. The resulting Δx depended on the linear scanning speed over a fix distance between the fiber and sample. On the other hand, the pixel size in y-direction (Δy) was limited by the shift in y-direction by the motorized stage, fixed at 0.05 mm in this current study. To test the effect of linear scanning speed on the pixel size in reconstructed FLIM, a series of scanning measurements on the physical phantom (Phantom 1) with scanning speeds of 0.1 mm/s, 0.2 mm/s, 0.4 mm/s and 1 mm/s were performed. The fiber tip was kept at 1 mm above the scanning surface. The images were recorded in channel 4 corresponding to the RhB emission.

#166495 - $15.00 USD Received 13 Apr 2012; revised 25 May 2012; accepted 25 May 2012; published 6 Jun 2012

2.3.2 Pixel size in helical scan

In helical scan, the scanning speed was controlled by two parameters, i.e., fiber rotation speed and pullback speed (speed along vessel axial direction). The pixel size along the circumferential direction (Δx) is the scanning distance along the circumference within the time interval needed to acquire and store a fluorescence decay curve. For a fixed angular velocity (e.g., 20 revolutions per minute - RPM), Δx depends on the diameter of the vessel. The pixel size along axial direction (Δy) is the pullback distance within the time interval of one fiber rotation. In this study, these two parameters were fixed at 20 RPM and 0.04 mm/s respectively.

To test the effect of vessel diameter, a series of scan measurements were repeated in helical scan mode on acrylic tubes with lumen diameter of 2, 4 and 6 mm in a physical phantom (Phantom 2). The scanned segment was 2.4 mm along the lumen.

2.3.3 Spatial resolution

The smallest target the scanning system can resolve was determined by measuring fluorescence responses from a sharp-tipped phantom (Phantom 3) in the linear scan mode. In this experiment, the linear scanning speed was adjusted to 0.05 mm/s and the fiber-to-sample distance was set at 0.3 mm above the sample. Since this working distance provides a near contact of probe with tissues, such measurement provides an estimate of the best resolution that can be achieved using the current optical configuration. The spatial resolution is expected to be affected by the fiber (light beam), scanning speed, and the fiber-to-sample distance, which affects the beam size at the sample surface.

2.3.4 System validation

The scanning system with helical scanning was validated using both the physical phantom (Phantom 4) and the hybrid pig aorta phantom. The scanning parameters were 20 RPM along the radial direction and 0.04 mm/s pull-back speed along the axial direction. The scanned segment was ~8 mm long in the lumen, the image maps consist of 88 x 120 pixels at 0.21 x 0.11 mm pixel interval. In current configuration, the total data acquisition time was relatively long (~4 minutes) due to the low repetition rate of the laser (30 Hz). Fluorescence signals were acquired from four spectral channels and subsequently analyzed to generate the 2D image of integrated intensity and average lifetime images.

2.4 Data processing

For each of the four spectral channels, the set of fluorescence decays were analyzed to generate both 2D fluorescence intensity images and lifetime images. The value of each pixel on an intensity image was produced by integrating as a function of time the fluorescence decay measured from the corresponding location. The integrated intensity image represents the relative intensity of fluorescence emission at each pixel. The average lifetime image is the spatial distribution of decay time constants retrieved from the fluorescence decays across the scanning area. Since the measured fluorescence decay is a convolution of intrinsic fluorescence response of the fluorophore to an impulse excitation and the impulse response of the instrumental system, the fluorescence decay was deconvolved by using a fast least-square deconvolution technique based on Laguerre basis function expansions as previously reported [22,23]. The corresponding average lifetime was then calculated as the mean decay time of the deconvolved fluorescence decay function [22]. Data were analyzed using Matlab (Matlab R2009b, Mathworks, Inc.).

#166495 - $15.00 USD Received 13 Apr 2012; revised 25 May 2012; accepted 25 May 2012; published 6 Jun 2012

3. Results

3.1 Characterization of the scanning TRFS system

3.1.1 Effect of scanning speed on pixel size: evaluation using the linear scan

Figures 2(a) and 2(b) show the integrated intensity and average lifetime maps from the 630 nm fluorescence spectral band. Pixel size and averaged lifetime value at each scanning speed are summarized in Table 1. Fluorescence data was collected from areas of 3 x 1.5 mm^2 (75x30 pixels).

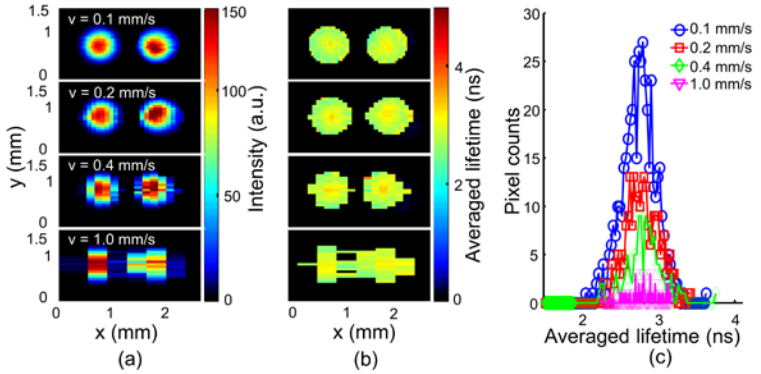

Fig. 2. Effect of scanning speed on pixel size and reconstruction of fluorescence intensity and lifetime imaging maps. 2D- maps of fluorescence intensity (a) and lifetime (b) are given for a linear scan performed at 4 distinct scanning speeds. The FLIM images were acquired from RhB solution placed in capillary tubes positioned at 0.5 mm apart. (c) Histogram of average lifetime values corresponding to FLIM images in (b).

Table 1. Linear scan pixel sizes

Linear scan speed (mm/s)	**Pixel size (**$\Delta x \times \Delta y$**) (mm)**	**Lifetime (ns)**
0.1	0.04 × 0.05	2.65 ± 0.18
0.2	0.08 × 0.05	2.70 ± 0.21
0.4	0.16 × 0.05	2.72 ± 0.24
1.0	0.40 × 0.05	2.71 ± 0.27

The average lifetime values retrieved for each scanning speed were found consistent across all scanning speeds (Table 1), while the image quality degraded as the scanning speed increased from 0.1 to 1 mm/s. Figure 2(c) shows the histogram of lifetime corresponding to the lifetime image in Fig. 2(b). This test demonstrated that based on current system configuration, good spectroscopic images can be acquired at scanning speed of less than 0.4 mm/s. The signal-to-noise ratio of this experiment was ~40 dB.

3.1.2 Effect of vessel diameter on pixel size: evaluation using the helical scan

The pixel sizes and averaged lifetime at each scanning speed are summarized in Table 2.

Table 2. Helical scan pixel sizes (constant pullback speed at 0.04 mm/s and RPM at 20/s)

Diameter (mm)	**Pixel size (**$\Delta x \times \Delta y$**) (mm)**	**Lifetime (ns)**
2	0.07 x 0.11	2.51 ± 0.25
4	0.14 x 0.11	2.74 ± 0.21
6	0.21 x 0.11	2.53 ± 0.29

Figures 3a and 3b show the fluorescence of RhB at 630 nm spectral band projected along a cylindrical geometry. The image maps consist of 88 x 22 pixels. As lumen diameter increased,

#166495 - $15.00 USD Received 13 Apr 2012; revised 25 May 2012; accepted 25 May 2012; published 6 Jun 2012

the intensity of fluorescence emission decreased with increasing (circumferential) pixel size. Note that since no fluorescence pulses were averaged using FastFrame in the helical scan, the lifetime maps had high variability as a result of low signal-to-noise ratio (SNR). Figure 3d shows the histogram of average lifetime values for different diameters. The normalized intensity profiles (NIP) along the center of the phantom at different lumen diameters are shown in Fig. 3c. The full width half maximum (FWHM) of the NIP for the 6 mm lumen diameter showed that the images of the two separate fluorophores overlapped. This indicated that the increase in lumen diameter reduced the ability of differentiating the two fluorophores due to the subsequent increase in beam size and pixel size.

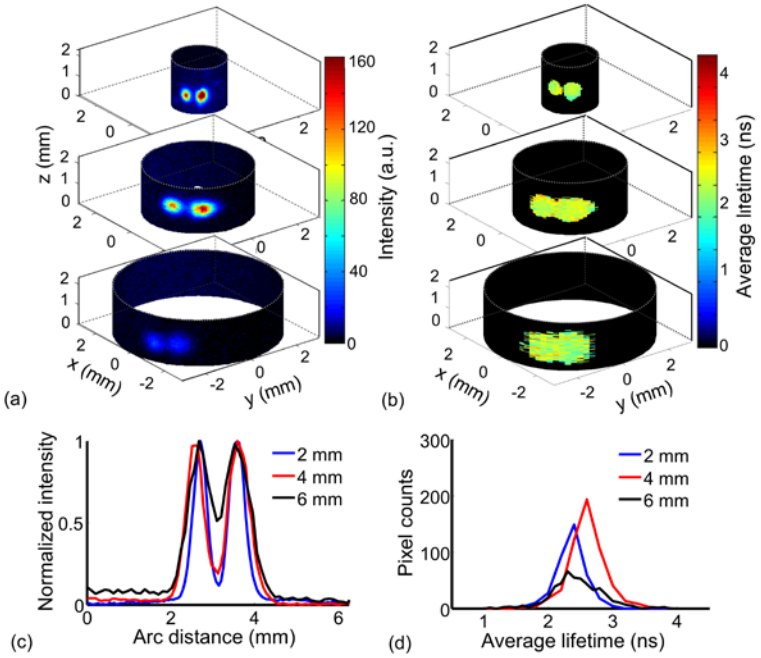

Fig. 3. Effect of lumen diameter (acrylic tubes) in helical scan on pixel size and reconstruction of fluorescence intensity and lifetime imaging maps. The optical fiber was centered in the acrylic tube resulting in distances between the fiber tip and fluorophore on the lumen wall was determined by the acrylic tubes with diameter of 2 mm, 4 mm and 6 mm respectively. The helical scan of 2D- fluorescent intensity (a) and lifetime (b) imaging maps (in loop format) was measured from fluorophores pair (RhB) separated by 0.5 mm along luminal circumference. (c) The intensity profile along the center of fluorophore phantom as a function of arc distance. (d) The histogram of average lifetime values corresponding to lifetime maps in (b).

3.1.3 Evaluation of spatial resolution using the linear scan

Figure 4(a) shows the geometry of the needle-shape capillary phantom. In Figs. 4(b) and 4(c), the integrated intensity and average lifetime images have a similar shape as the capillary tip. Figure 4(d) depicts the NIP along capillary cross-section at different diameter (L1-L7). The smallest FWHM of the NIP is ~250 μm at the tip diameter of 80 μm. Specifically, the cross-section lines for diameters less than L4 the NIPs had similar shape and FWHM. Thus targets with the width less than the diameter of L4 were un-resolvable with the current system. Consequently, NIP (with FWHM ~250 μm) from L1-L4 provides the system point spread function. The pixel size of this measurement was 20 μm in x-direction and 25 μm in y-direction.

#166495 - $15.00 USD Received 13 Apr 2012; revised 25 May 2012; accepted 25 May 2012; published 6 Jun 2012

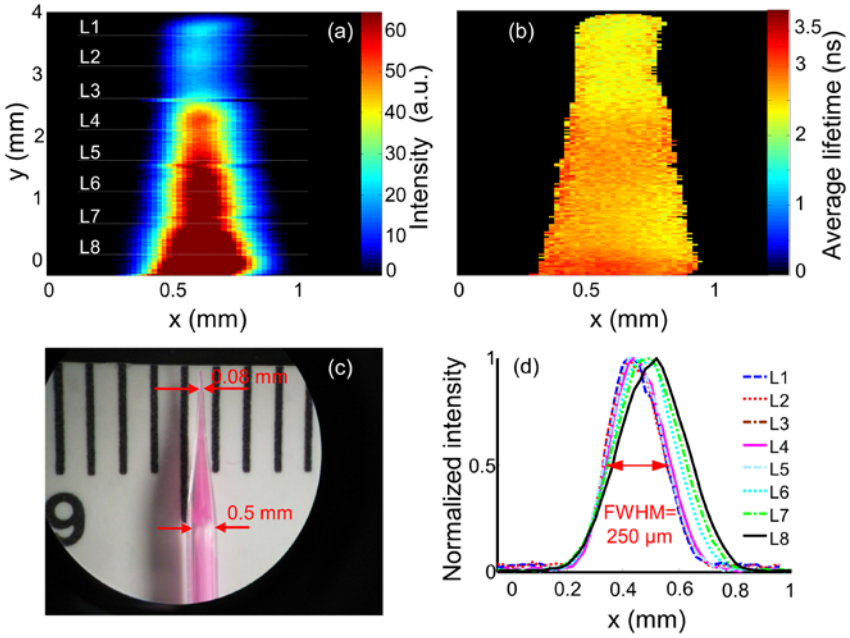

Fig. 4. Evaluation of the spatial resolution of the scanning-TRFS system (results from linear-scan). Fluorescence images of RhB dye placed in a needle-shape capillary: (a) Fluorescent intensity (b) lifetime map (FLIM); (c) Photograph of the needle-shape capillary with diameter varied from 0.08 to 0.5 mm; Note the shape of the fluorescence emission follows the shape of the capillary; (d) Normalized intensity profiles along lines L1-L8 as depicted in (a). The interval in y-direction between the lines (L1-L8) is equal to 0.5 mm along the fluorophore at the position of different diameter. The spatial resolution of the scanning TRFS system was determined as 250 μm by the FWHM of point spread function (i.e., the intensity profile at the sub-resolution 80 μm capillary tip).

3.2 Validation of the system in helical scanning

3.2.1 Resolving fluorophores in physical phantom

The performance of the scanning-TRFS system in helical scanning was validated using the physical phantom (Phantom 4) that allows for testing of the system ability to simultaneously resolve the spectral and temporal emission of multiple fluorophores [Fig. 5(c)]. Figures 5(a) and 5(b) depict the fluorescence intensity and lifetime maps obtained from this phantom. For example, the narrow band fluorescence emission of RhB (peak emission 630 nm) was observed at the spectral band of 630 nm (channel 4). The overlapped emission of C120 and C1 was observed in channels 1 and 2 while the emission of FITC was primarily observed in channels 2 and 3. Four fluorophores (C1, C120, FITC and 9CA) presented a spectral overlap in channel 2 [Figs. 5(a), 5(b)]. Except for C120 and FITC which have very similar lifetimes (~3.8 ns, ~3.56 ns, respectively), the scanning-TRFS system was able to resolve the fluorescence emission these fluorophores in the time-domain as depicted by their average lifetime histogram [Fig. 5(d)]. The emission peaks, and means of average lifetimes of C120, C1, 9CA, FITC, and RhB of each fluorophores comparing to literature value are summarized in Table 3. While absolute comparisons with the values reported in the literature are difficult to make due to the dependence of the solvent, viscosity or parameters of the environment, these results were in agreement with previously reported values [24]. Overall, these results demonstrate that a combination of both spectral and time-resolved fluorescence features can be used to resolve the fluorescence emission of multiple fluorophores.

#166495 - $15.00 USD Received 13 Apr 2012; revised 25 May 2012; accepted 25 May 2012; published 6 Jun 2012

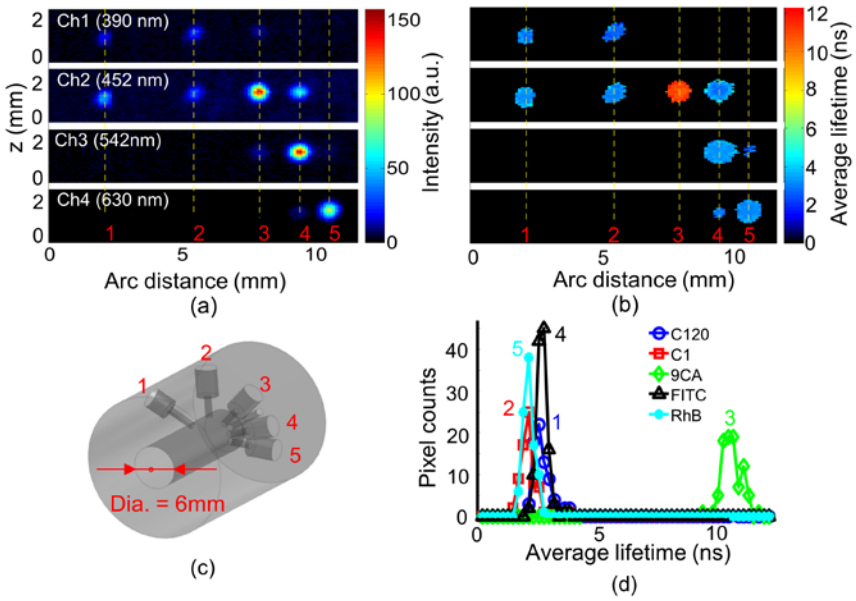

Fig. 5. Scanning-TRFS system ability to spectrally and temporarily resolve the fluorescence emission of five distinct fluorophores (1) C120, (2) C1, (3) 9CA, (4) FITC, and (5) RhB contained in the radial tubular/capillary structures. Validation in a cylindrical physical phantom for the four wavelength bands/channels. (a) Fluorescence intensity in 2D open-format depicting the channels where each fluorophore fluoresces; (b) lifetime imaging maps in open-format depicting the resolved average lifetimes for each fluorophore. (c) Schematic of the 6 mm diameter acrylic tube phantom with the five radial tubes in which the fluorophores are placed and labeled as position 1 to 5. (d) Histogram of average lifetime corresponding to the lifetime imaging maps presented in (b).

Table 3. Fluorescence characteristics of fluorophores used in physical phantom

Fluorophores	Emission Peak (nm)	Lifetime (ns)	Literature emission (nm), lifetime value (ns)
C120	430	3.38 ± 0.31	430, 3.64 [17]
C1	450	2.96 ± 0.33	450, 3.1 [18]
9CA	445	11.00 ± 0.33	445, 11.9 [19]
FITC	540	3.56 ± 0.25	540, 3.6 [20]
RhB	600	2.70 ± 0.22	600, 2.5-3.0 [16]

3.2.2 Resolving fluorophores in ex vivo hybrid pig aorta phantom

Figure 6 shows the fluorescence maps of the pig aorta phantom vessel wall in a closed-loop [Fig. 6(a)] and open-loop [Fig. 6(c)] image format. The application of the rotational SVOF in a ~6 mm diameter pig aorta is depicted in [Fig. 6(b)]. The structure of the stent was clearly seen against the autofluorescence background (in channel 1 of 390 nm and channel 2 of 450 nm) originating from the aorta wall [Figs. 6(a) and 6(c)]. This broad emission (370-500 nm) with a relative long average fluorescence lifetime of ~5 ns [Fig. 6(d)] was clearly observed in the corresponding emission channels (Channels 1 and 2), and is attributed to the emission of structural proteins in the arterial wall (elastin and collagen). Elastin, in particular, is known to be the dominant contributor of fluorescence signal in the normal aorta upon UV excitation [9,10]. The fluorescence emission of C1 bead placed on the stent was spectrally and temporally-resolved in channels 1 (390 nm) and 2 (450 nm). Although the bead intensity was found to be significantly lower in channel 1 than channel 2, the average lifetime values in this two channels were similar (~3.0 ns) and in agreement to the reported C1 average lifetime fluorescence. As expected, the fluorescence emission of FITC-based bead was resolved in

#166495 - $15.00 USD Received 13 Apr 2012; revised 25 May 2012; accepted 25 May 2012; published 6 Jun 2012

channel 3 (average lifetime ~3.6 ns). The fluorescence of the Rhodamine-based reference marker was also resolved in channels 3 and 4 (average lifetime ~3.0 ns) as expected. Examples from two locations of the phantom demonstrating the accuracy of deconvolution are depicted in Figs. 6(e) and 6(f). One location corresponds to C1 with an average lifetime of 2.74 ns [Fig. 6(e)]. The second location corresponds to the normal vessel wall showed a longer lasting average lifetime of 5.43 ns [Fig. 6(f)].

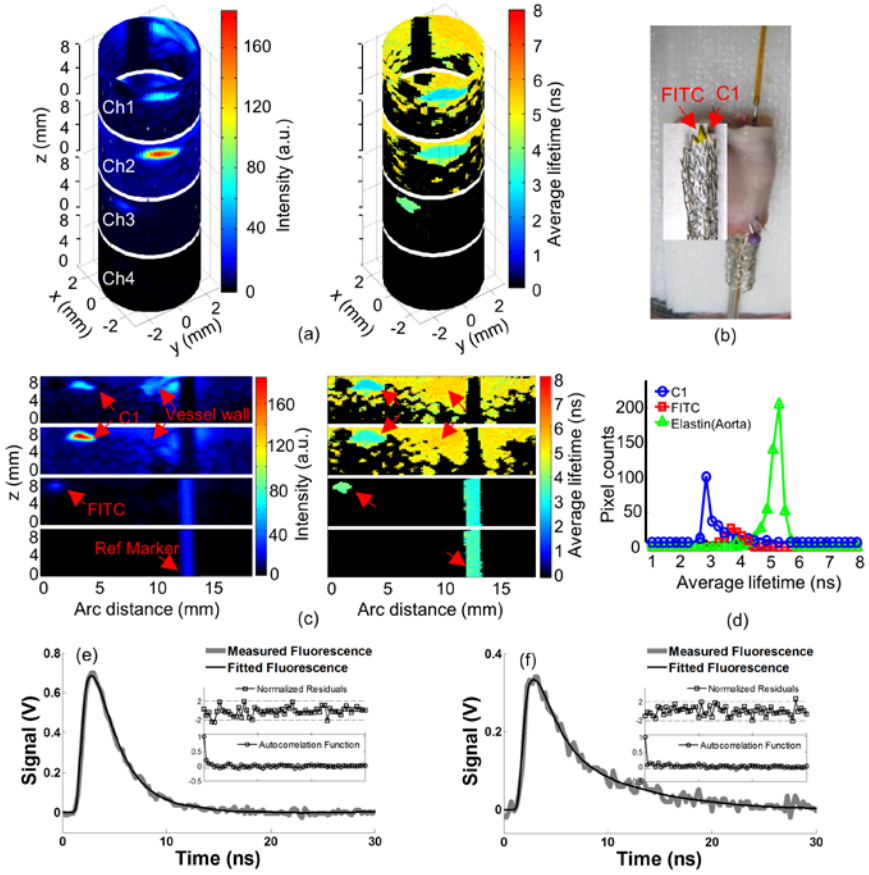

Fig. 6. Scanning-TRFS system ability to spectrally and temporarily resolve the fluorescence emission of target fluorophores placed in arterial lumen. Validation in an intact pig aorta tissue with target fluorophores placed on a metallic stent. (a) Fluorescence intensity in close-format (upper) and open-format (button) depicting the channels in which each target fluorophore fluoresce; (b) Lifetime imaging maps in close-format (upper) and open-format (button) depicting the resolved average lifetimes for each fluorophore; (c) Application of fiber-optic probe in the pig aorta phantom (inner diameter/lumen: ~6 mm) with stent deployed inside. Two fluorophores: C1 and FITC mounted on the stent are shown in the inset photo. The third fluorophore (RhB) not seen in the picture acted as reference marker. (d) Histogram of average lifetime corresponding to the vessel wall autofluorescence generate by structural proteins and C1 and FITC-based beads. Note that the stent wire can be distinguished against the aortic wall autofluorescence (Channels 1 and 2). The fluorescence of the fluorescence beads is also resolved against the aortic wall autofluorescence: C1 in channel 1 and 2 and FITC in channel 3. The fluorescence emission of the reference marker (RhB) is observed in channels 3 and 4. (e) and (f) Examples from two locations in the phantom on the phantom demonstrating the accuracy of deconvolution between the measured fluorescence pulse and fitted fluorescence pulse, the residuals between these two, and the correlation of residuals: (e) one location from the dye C1 (x = 3.78 mm y = 5.5 mm); (f) second location from the vessel wall (x = 10.3 mm y = 5.5 mm). Both signals are from the channel 1.

#166495 - $15.00 USD Received 13 Apr 2012; revised 25 May 2012; accepted 25 May 2012; published 6 Jun 2012

4. Discussion and conclusions

This study demonstrates the novel application of a fiber-based point-spectroscopy TRFS system to record fluorescence data in a continuous helical scanning (radial) manner across multiple spectral emission bands; and to accurately reconstruct and resolve fluorescence lifetimes of fluorescent targets located on tubular structures (e.g., luminal surface of arterial wall). The performance of the scanning-TRFS system to create FLIM images (including the image pixel size, data acquisition speed, SNR, and accuracy of lifetime values) were found to depend on a range of the experimental parameters such as laser repetition rate, average number of fluorescence pulses to improve SNR, beam size, scanning speed, lumen diameter, bandwidth and speed of the digitizer, response time and sensitivity of the detector. These are discussed in the following. Based on current results, optimized imaging parameters can be determined for specific application in subsequent studies.

As anticipated, the evaluation of the effect of the scanning speed on the pixel size showed that the lower scanning speed results in smaller pixel size (0.04 mm pixel size with 0.1 mm/s versus 0.4 mm with 1 mm/s) and thus improved image quality. However, this is at the expense of increased data acquisition time ranging from a few to several minutes. For the scanning-TRFS system described here using the digitizer's build in FastFrame data acquisition mode, the laser repetition rate is the major limiting factor in improving the scanning speed while preserving the image quality. The current averaged acquisition time per pixel is ~0.4 s, which includes the time needed for averaging of 6 consecutive pulses at 30 Hz, data processing, displaying, and storing data. Currently, it takes 1 to 15 minutes to record a FLIM image, depending on the size of scanning area. The acquisition time can be significantly reduced by using a fast repetition rate laser. We anticipate that use of pulse rate at 10 kHz combined with the same FastFrame data acquisition mode can reduce this scanning time from minutes to a few seconds.

The spatial resolution of the scanning TRFS system was mainly determined by the size of the optical beam at the tissue/sample surface and light excitation-collection geometry (fiber-to-tissue distance). As demonstrated by the experiments concerning the effect of vessel diameter on the ability to resolve two fluorophores in the fluorescence image (Fig. 3), the increased working distance due to a large lumen diameter resulted in not only a larger pixel size (0.07 mm for 2 mm vessel versus 0.21 mm for 6 mm vessel) but also reduced spatial resolution. The current system resolution, which was characterized as ~250 μm by measuring the point spread function (Fig. 4), can be improved by decreasing the numerical aperture of the fiber optic or by increasing the refractive index of the media in the biological application in which the laser beam travels through. Inherently, applications in an intravascular settings will benefit from the latter since the spatial resolution could be improved in the water/saline environment ($n = \sim 1.3$) compared to air ($n = 1.0$).

An important feature of the scanning-TRFS system described here is its ability to simultaneously resolve the fluorescence intensity decay in multiple spectral bands. The current system allows for spectral separation of all fluorophores used in the validation tests (Figs. 5 and 6). Each of the fluorescent structures (e.g., Figure 5) can be clearly observed in distinct spectral channels in various intensity scales. Moreover, overlap in spectral emission of the fluorescent structures can be further delineated using time-resolved measurements (e.g., C120 and C1). Overall, current results demonstrate that this system is capable of resolving the fluorescence decay of most fluorescent components in biological tissue with lifetimes ranging from 2 ns to 12 ns in a broad spectral band ranging from about 370 nm to 650 nm. While certain spectral bands were used in this study, the modular design of current instrument enables selection of any spectral band of interest by simply replacing the set of dichroic filters and band-pass filters within the wavelength selection module (Fig. 1).

One of the goals in the development of the scanning-TRFS system is to ultimately apply such a system in clinical cardiovascular diagnosis. This study not only has demonstrated that

#166495 - $15.00 USD Received 13 Apr 2012; revised 25 May 2012; accepted 25 May 2012; published 6 Jun 2012

such approach can facilitate robust and continuous TRFS data acquisition from the arterial lumen, but also the identification of fluorescent molecular structures with distinct fluorescence lifetime against the autofluorescence emission of normal arterial wall. For atherosclerotic plaque characterization and diagnosis, it is important to differentiate molecular composition within the vessel wall (i.e., elastin, collagen and lipids) that are associate with distinct plaque pathological features. The hybrid tissue phantom, including pig aorta, fluorophore dyes, and a stent, enabled evaluation of a few conditions that are useful for future practical implementation of this technique. For example, the tests conducted in this phantom showed that the scanning-TRFS system is sensitive enough to resolve the autofluorescence emission of the normal arterial wall. While the fluorescent dyes used to generate fluorescent targets cannot mimic entirely the fluorescence emission of lipid-rich atherosclerotic plaques, they allowed for testing whether the emission of molecular structures with different decay dynamics than the normal arterial tissue can be resolved. The reconstructed fluorescence lifetime revealed that fluorescent targets with shorter lifetime values (~3 ns) than the aorta autofluorescence (~5 ns) can be distinguished from normal aortic tissue (Fig. 6). Since lipid-rich plaques were shown to exhibit faster decay dynamics than normal arterial wall rich in elastin and collagen [8,9], current results demonstrate that the scanning-TRFS has the potential to localize such plaques that are associated with critical cardiovascular events. The use of the stent allowed observation of the scanning system to resolve nonfluorescent structures within the vessel wall.

Moreover, the fiber optic-based rotational scanning system allows for further integration of this device coupled to other intravascular techniques such as intravascular ultrasound (IVUS) [25]. Such bi-modal system can provide a simultaneous characterization of both biochemical and structural characteristics of the atherosclerotic plaques. A few approaches for coupling these two modalities were described in our earlier publications [11,13,26]. When applied synchronously, IVUS not only can provide structural information on the vessel wall but also information on the lumen diameter and the position of the optical fiber relative to the vessel wall. Based on the information on the lumen diameter acquired by IVUS, the pixel size and fluorescence signal can be corrected to reconstruct the FLIM images in cases where the size of the lumen in not uniform or the fiber is not at the centered in the lumen. The fluorescence intensity variation due to changes distance between the tip of the fiber and vessel wall is less of a concern for time-resolved fluorescence measurements, as the information derived from these measurements is primarily based on the analysis of the fluorescence decay dynamics rather than absolute intensity. Developments in this direction are currently pursued by our group.

In conclusion, we demonstrated the feasibility of a prototype scanning-TRFS system with fiber optic for performing a helical scan to acquire intraluminal FLIM data. The scanning system was validated by recording the fluorescence signals in a continuous data acquisition sequence using *in vitro* physical phantoms and a hybrid *ex vivo* pig artery phantom. The performance of the scanning TRFS system was characterized with multiple experimental settings including different scanning speeds and lumen diameters in a vessel phantom. The robust fluorescence lifetime retrievability during scanning-TRFS measurements suggests a great potential for application of this scanning system for intravascular cardiovascular diagnosis. The use of high repetition laser devices (e.g., Fianium fiber laser with repetition rate up to 20 MHz) along with advancement of new solutions for continuously removing the blood from the optical pathway as recently reported [26] is anticipated to facilitate development of the next generation of scanning-TRFS systems and *in vivo* FLIM-based characterization of plaque cap composition during intravascular interventions.

Acknowledgments

This work was supported by NIH Grant R01HL067377.

#166495 - $15.00 USD Received 13 Apr 2012; revised 25 May 2012; accepted 25 May 2012; published 6 Jun 2012